DEUTSCHES ELEKTRONEN-SYNCHROTRON DESY

DESY 70/14
March 1970

Optical Properties of the Rubidium- and Cesium-Halides in the Extreme Ultraviolet

M. Cardona, R. Haensel, D.W. Lynch, and B.Sonntag
Deutsches Elektronen-Synchrotron DESY, Hamburg, Germany

and

II. Institut für Experimentalphysik der Universität Hamburg
Hamburg, Germany

2 HAMBURG 52 · NOTKESTIEG 1

Optical Properties of the Rubidium- and Cesium-Halides in the Extreme Ultraviolet[†]

M. Cardona[††], R. Haensel, D.W. Lynch[†††], and B. Sonntag

Deutsches Elektronen-Synchrotron, Hamburg, Germany

and

II. Institut für Experimentalphysik der Universität Hamburg

Hamburg, Germany

The absorption spectra of evaporated thin films of all Rubidium- and Cesium-Halides in the 50 to 250 eV region are reported. In this range transitions from the 3d-shell of Rb^+ and from the 4d- and 4p-shell of Cs^+ can be seen, as well as some transitions from inner shells of the halogen ions. Besides the absorption fine structure near the threshold for inner shell transitions, broad absorption structure is observed and explained as due to d→f continuum transitions. The number of effective electrons, whose oscillator strength has been exhausted in our spectral region has been computed from the absorption data: it is particularly strong for materials containing either Cs or I. Differences in the spectra of materials with NaCl and with CsCl structure are discussed. The measurements were performed using the DESY electron synchrotron as a light source.

[†] Work supported by the Deutsche Forschungsgemeinschaft

[††] John S. Guggenheim Memorial Foundation Fellow, on leave from Brown University, Providence, Rhode Island

[†††] present address: Iowa State University, Ames, Iowa

I. INTRODUCTION

The electronic optical properties of the alkali halides have been studied experimentally and theoretically for many years. These studies have been concerned both with the behavior of pure crystals[1] and with the additional effects produced by defects and impurities.[2] Most measurements were performed using conventional absorption techniques. Measurements of the spectral yield for photoelectric emission and the energy distribution of the photoemitted electrons have also contributed to our knowledge of the electronic structure of the alkali halides.[3] More recently transmission[4] and reflection[5] modulation experiments, and two-photon absorption spectroscopy[6] have appeared as valuable techniques for studying these materials.

The alkali halides consist of ions with closed outer electron shells and therefore the pure crystals (which will be exclusively considered in this work) only begin to absorb in the uv, at about 6 eV. LiF has actually a band gap of about 12 eV. Most of the reported measurements have been made in the uv and vacuum uv range up to 25 eV. They cover transitions with initial states in the valence bands (outermost shells of the halogen ions). Whereas the pioneering investigations of the Hilsch-Pohl school[7] were done by absorption spectroscopy of thin films recent measurements of the reflection spectra of single crystals[8-10] seem to show more details, thus indicating some sensitivity of the observed structure to crystalline perfection. Beside optical studies, electron energy loss measurements[11,12] also allow the evaluation of the optical constants of the alkali halides in the energy range up to 20 eV.

While simple charge-transfer models and atomic considerations were used for

the earlier interpretation of the experimental data, the recent availability of calculated band structures for the alkali halides makes a detailed interpretation of the observed spectra in terms of these band structures highly desirable. Such interpretation has proven very successful for covalent materials.[13] The existence of strong, clearly identifiable exciton effects at the threshold for interband transitions raises the question of how much of the observed optical behavior can be related to one-electron interband transitions. This question will not be answered until reliable calculations of optical constants from the one-electron band structure become available.[14] In the meantime, an attempt is usually made to classify the excitons into Wannier (hydrogenic) series tied to a given interband critical point. The onset of interband transition is then viewed as the convergence limit of the exciton series. Band calculations have been performed for RbF,[15] RbCl, RbBr,[16] RbI,[17] CsF[15,18] (all with the rock salt structure) and for CsI (both, with rock salt and with CsCl structure)[19,20]. All these calculation show the bottom of the conduction band at Γ. The wavefunctions at this minimum, with Γ_1 orbital symmetry (Γ_6^+ double-group symmetry) are mostly composed of s wave functions of the metallic ion. The top of the valence band occurs also at Γ; it has Γ_{15} orbital symmetry (Γ_8^- double group) and corresponds largely to p wave functions of the halogen ion. The spin-orbit splitting of the Γ_{15}states into Γ_8^- and Γ_6^- is close to the corresponding splitting of the halogen ion: approximately 0.05 eV for F^-, 0.1 eV for Cl^-, 0.5 eV for Br^-, and 1.0 eV for I^-. According to these considerations, the lowest-energy peak observed in the absorption spectrum of the Rb- and Cs-halides[8-10, 21-24] is generally

interpreted as an exciton formed from the upper (Γ_8^-) branch of the Γ_{15} valence bands and the bottom of the conduction band (Γ_6^+). In the fluorides the spin-orbit mates ($\Gamma_8^- - \Gamma_6^-$) are very close together and therefore the $\Gamma_8^- - \Gamma_6^-$ splitting cannot be resolved: in the chlorides this splitting can easily be seen at low temperatures. In reflection measurements on single crystals of the bromides and iodides, a much smaller second peak has been recognized after the first peak;[8-10] it has been interpreted as the n=2 member of a Rydberg series[25] associated with the $\Gamma_8^- - \Gamma_6^+$ band edge:

$$E_n = E_o - \frac{G}{n^2}, \qquad n = 1, 2 \ldots$$

E_n being the energy of the n-th exciton, E_o that of the series limit (the band gap energy) and G the binding energy of the first exciton. The observation of higher (n>2) excitons in thin film absorption has only been possible for RbI.[24] In contrast, for the solid rare gases[26-28] materials with otherwise similar optical properties, exciton series with members up to n=4 have been easily observed.

For the bromides and iodides the spin-orbit splitting is big enough to shift the $\Gamma_6^- - \Gamma_6^+$ exciton into a region where other peaks, apparently not related to the $\Gamma_{15} \rightarrow \Gamma_1$ edge, can be seen. In this case the identification of the high energy component of the $\Gamma_{15} - \Gamma_1$ exciton among the other neighboring structures is not always unambiguously possible. For instance in RbI Baldini and Bosacchi first interpreted a peak at 6.6 eV as an exciton[8], related to band edges at X and later as a spin-orbit mate of the $\Gamma_8^- - \Gamma_6^+$ exciton[9], because of its temperature behavior.[23] The original identification of excitons tied to interband critical points at L made by

Phillips[29] seems to have been abandoned in favor of X excitons. Fröhlich and Staginnus[6] have been able to identify with the aid of two-photon spectroscopy excitons related to the lowest X critical point in CsI (with CsCl structure). Such transitions are forbidden in conventional one-photon spectroscopy because of parity;[19] they become allowed as two-photon transitions since the parity selection rule is reversed (initial and final states must have the same symmetry). The two-photon X exciton occurs at 6.25 eV in CsI, between the $\Gamma_8^- \rightarrow \Gamma_6^+$ and its spin-orbit mate ($\Gamma_6^- \rightarrow \Gamma_6^+$). The $\Gamma_8^- \rightarrow \Gamma_6^+$ interband transition is forbidden for two photons, but it becomes weakly allowed when considered as an exciton for $n \geq 2$: as such it has also been observed in 2-photon spectroscopy. The 2-photon absorption edge is shifted with respect to the 1-photon edge by the n=1 - n=2 exciton energy difference.

The bulk of optical measurements existing in the literature has been performed from the absorption edge up to about 12 eV. Measurements up to 35 eV have been reported by Saito et al.[30] One can see in the Rb-halides at 16 eV the onset of transitions from the outermost Rb^+ (4p-) shell, in the Cs-halides at 13 eV the onset of transitions from the outermost Cs^+ (5p-) shell, the peaks are however imbedded in a continuum due to the higher valence bands and unambiguous assignment to the different initial states is difficult. The identification of the onset of the Rb^+ (4p) and the Cs^+ (5p) transitions at 16 eV and 13 eV agrees with the known energies for the first excitation of the free ions.[31] Measurements of transitions from the outermost Na^+ (2p) transitions in the Na-halides[32] and the outermost Li^+ (1s) transitions in the Li-halides[33] also give energies in agreement with the onset of transitions in the free ions, i.e. 32.5 eV for Na^+ and 60 eV for Li^+. The limitation in the

resolution of measurements above 10 eV, such as those of Saito et al.[30], is due to the sources commonly used in these experiments. The source problems become more and more severe the higher the photon energy. The intensity of discharge sources usually decreases with increasing photon energy; the line density of multiline sources becomes smaller. For measurements in the photon energy range above 10 eV the ideal source is the synchrotron radiation from high energy electron synchrotrons and storage rings.[34]

In this paper we report the absorption spectra of the Rb- and Cs-halides between 50 and 250 eV. As shown in Fig. 1, mainly transitions with initial states at the outermost d-subshells of Rb^+, Cs^+, Br^-, and I^- are expected in this photon energy range. We have also observed transitions from the p-levels of the same shell of Cs^+. The samples were thin films vacuum deposited onto thin carbon substrates: It is not possible to obtain single crystals thin enough to perform absorption measurements in this region. While single crystal measurements would be possible by reflection, the reflectivity of the alkali halides between 50 and 250 eV is too small (< 1 %) to perform accurate measurements. Consequently reflection corrections can be neglected in transmission work. From our knowledge of the width of the valence excitons in thin films, it is possible to say that the width of the rather broad peaks observed between 50 and 250 eV is not due to crystalline disorder. Absorption measurements should also be more accurate in this region than electron energy loss measurements. The latter become preferable in the neighborhood of the plasma frequency of the valence electrons ($\sim$ 15 eV) because of the small values of the dielectric constant: energy loss measurements give essentially the function $\frac{1}{\epsilon}$.

In the next section details of the experimental arrangement are given. Section III gives the results of the measurements and section IV a discussion of the fine structures near theshold as well as of the characteristic continuum absorption related to the so called delayed onset of the d→f transitions.

II. EXPERIMENTAL PROCEDURE

The thin film absorption measurements were performed using the 7.5 GeV electron synchrotron DESY as radiation source.[36] The experimental arrangement is described to some extend elsewhere.[37] The light coming from the synchrotron passes through a beam-pipe of approximately 40 m length and is then focused by a concave mirror into the entrance slit of a grazing incidence monochromator. For the measurements between 50 and 200 eV a gold-coated grating with 2400 lines/mm and a blaze angle of $4^{o}16'$ was used in first order with an angle of incidence of $12^{o}30'$. An Al filter was used to cut off higher spectral orders below 72 eV. For the range between 150 and 250 eV a 3600 lines/mm grating was used with a blaze angle of $3^{o}8'$ and an angle of incidence of $3^{o}50'$. The wavelength resolution of the instrument was 0.1 Å over the entire energy range. The detector was a Bendix M 306 open magnetic electron multiplier.

The signal from the photomultiplier, placed behind the exit slit, was fed into the Y channel of a XY potentiometric recorder whose reference signal was proportional to the current in the accelerator, thus compensating current fluctuations. The X axis of the recorder received a voltage from a potentiometer linked to the wavelength drive of the monochromator. The samples were mounted in front of the focusing mirror. Some samples were prepared by evaporation from Al_2O_3-covered molybdenum baskets in situ, while others were prepared ex situ and then transferred to the sample chamber. In situ preparation was especially convenient for the very hygroscopic materials such as RbF and CsF. With both preparation methods the film thickness was determined with an oscillating quartz[38] calibrated by Tolansky interferometry. The accuracy of the thickness determination is estimated to be about ±20 %.

No differences have been found for samples prepared by either procedure provided the samples deposited ex situ are kept exposed to the atmosphere only for a short time. The substrates were carbon foils of ∿500 Å thickness[39] supported by a 75 µm copper grid. Best results were obtained with samples which transmitted about 10 to 50 % of the incident light. If the samples are too thick, the influence of stray light, higher spectral orders, and pin holes causes errors. Since the absorption coefficient near thresholds of inner shell transitions and near broad d→f peaks are different, samples of different thicknesses, ranging from 100 Å to 10000 Å, had to be used to obtain uniform accuracy. The consistency of the results for samples of different thickness was always checked. All measurements were performed at room temperature.

For measurements of samples evaporated in situ, the transmission of the carbon substrates was measured before the evaporation. With samples evaporated ex situ, the transmission of another similar carbon film was used as reference. The X-Y recorder plots were digitalized and computer processed so as to obtain the absorption coefficients shown in Figs. 2 - 10. The absolute error in the absorption coefficient curves is about ±20 %, mostly due to uncertainties in the sample thickness. The relative consistency of the values in adjacent regions is about ±3 % due mostly to incomplete compensation of synchrotron fluctuations by our recording system.

III. EXPERIMENTAL RESULTS AND DISCUSSION

a) General Review of the Absorption Curves

Rb-Halides

Figures 2 - 5 show the absorption spectra of all Rb-Halides in the energy range from ∿50 to ∿180 eV. The onset of Rb^+ 3d- transition (for reasons of convenience we use both the atomic and the X-ray nomenclature for the different subshells: i.e. $N_{IV,V}$ ∿4d, $N_{II,III}$ ∿4p, $M_{IV,V}$ ∿3d and $M_{II,III}$ ∿3p) can be seen by the appearance of fine structure near 110 eV. In RbF (Fig. 2) and RbCl (Fig. 3) the fine structure is sitting on an absorption continuum, which must still be due to transitions of outer electrons (valence band , Rb^+ 4p and 4s shells) into higher energy states of the conduction band.

The additional absorption due to transitions from the 3d-shell reaches in the first maxima about 30 % of that in the underlying continuum. The fine structure region extends over about 20 eV followed by an increasing absorption continuum with a maximum at about 150 eV. At higher energies the absorption begins to decrease again. This behavior is very similar to what has been found for the 3d-transitions of solid Kr.[40] This continuous absorption, which follows the fine structure near threshold can be explained as a delayed onset of d→f transitions.[41] The atomic potential caused by a superposition of the central potential of the core (appropriately screened Coulomb potential) and the centrifugal $l(l+1)/r^2$ term in the radial wave equation gives a potential barrier between bound and free states which suppresses d→f transitions near threshold and shifts their oscillator strengths to higher energies. The effect is especially pronounced for the 4d-transitions, as we will see later.

In RbBr the Rb^+ 3d-transitions at 110 eV (B_d^+, C_d^+, ...) are proceeded by the Br^- 3d-transitions (A_d^-, B_d^-, ...) which have their threshold at 70 eV. Since the Br^- 3d-transitions also have a delayed d→f onset, the Rb^+ 3d-fine structure takes place on an increasing absorption continuum. It should be noticed however that the oscillator strength of the Rb^+ 3d-peaks near threshold in RbBr is not smaller than in RbCl ($\sim 0.5 \cdot 10^4$ cm^{-1}). The superimposed maxima of the delayed d→f transitions of Br^- and Rb^+ are responsible for the broad maxima in the 130 to 150 eV region.

In RbI near 50 eV we see the onset of I 4d-transitions. The maximum of the d→f transitions is at about 95 eV and much stronger ($\sim 1.8 \cdot 10^4$ cm^{-1}) than for other Rb halides. If one assumes an oscillator strength of the Rb^+ 3d-peaks near threshold similar to that of RbBr and RbCl it becomes clear why it should not be detectable any more in the presence of the strong I^--continuum.

Cs-Halides

The corresponding spectra of the Cs-Halides are shown in Fig. 6 - 9. The Cs^+ 4d-threshold occurs at about 78 eV and can clearly be seen in CsF (Fig. 6) and CsCl (Fig. 7). As in the Rb-Halides the fine structure (A_d^+, B_d^+, ...) is superimposed on an absorption continuum of outer shell transitions. For all Cs halides we encounter 4d-transitions and, like in RbI, the continuum absorption above the Cs threshold is very strong (5×10^5 cm^{-1}). In CsBr (Fig. 8) we see first the Br^- 3d-structure (B_d^-, C_d^-, ...) near 70 eV followed by the Cs^+ 4d-structure at 80 eV. The absorption continuum of the 3d-transitions of Br^- does not influence much the Cs^+ 4d-absorption, in sharp contrast to CsI (Fig. 9) where the Cs^+

4d-threshold is sitting on the I 4d-continuum (threshold at 50 eV). Again the oscillator strength of the additional Cs^+ 4d fine structure in CsI is not smaller than in the other Cs-Halides but more difficult to detect because of the strong I^--continuum absorption on which it is superimposed. On the high energy side of the d→f peak we see another onset of fine structure due to transitions from the Cs^+ 4p-shell (A_p^+). Figures 6 - 9 only cover the spectral range up to 160 eV, where the onset of 4p-transitions takes place. Details of the Cs^+ 4p-structure at higher energies are given in Fig. 10. Measurements of CsCl[42] and CsI[43] have also been reported by F.C. Brown and coworkers. Their results are in good qualitative agreement with ours, although the oscillator strength in the d→f maxima near 110 eV are somewhat different. Stray light and higher spectral orders may be responsible for the discrepancy. The presence of stray light saturation in our results was ruled out by measuring a wide range of sample thicknesses: the spectra obtained for the thinner samples are essentially identical, while thicker samples show spurious saturation in the absorption.

The big oscillator strength in the delayed d→f maximum for 4d-transitions, and the comparatively smaller one for the 3d-transitions, has been discussed by Fano and Cooper.[41] It is sometimes called a resonance near threshold, which shows up as a concentration of the integrated oscillator strength above threshold; it is particularly strong if d→f transitions can take place within the same shell. This is obviously possible for 4d not for 3d transitions. The strong absorption continuum above threshold is about 80 eV wide for 4d-transitions but it is flattened and spread over a region of several hundreds eV for 3d-transitions. To check this more quantitatively we have evaluated N_{eff}, the effective number of

electrons whose oscillator strength is exhausted within the energy range covered by our measurements. It can be directly obtained from the absorption curves as

$$N_{eff} = 2.3 \cdot 10^{15}\ a^3 \int_{E_1}^{E_2} \mu\ (E) n(E) dE \ \text{(electrons/molecule)} \qquad (1)$$

Here n is the real part of the refractive index, which can be set equal to 1 in our energy region, as will be shown later, and a is the lattice constant. The N_{eff} for the different materials measured are summarized in Table I. For materials with only 3d transitions N_{eff} is small (between 1.3 for RbCl and 3.8 for RbBr), and agrees with the values found for solid krypton and for semiconductors[44] in the same spectral range. RbI, with 4d-transitions of I in our spectral range, has a considerably higher value of N_{eff}, indicating that most of the oscillator strength of the 4d-electrons is exhausted. The 4d-transitions of Cs seem to give an even higher value of N_{eff} (around 15 electrons/molecule). The contribution of both, 4d-transitions of Cs and of I, is reflected in the even higher value of N_{eff} for CsI ($N_{eff} \approx 18$). Similar results have been found for the 4d-transitions of Xe and of compound semiconductors.[44]

The coarse spectral dependence of the contribution of the transitions under consideration to the real part of the refractive index (Δn), as obtained from the Kramers-Kronig analysis of the data of Figs. 2 - 9, is represented in Table II. The contribution of transitions below 50 eV can be estimated with the standard free-electron expression $\left(n = -\omega_p^2/\omega^2\right)$; it is also small. As suggested earlier, n can be taken equal to one for the purpose of evaluation Eq. (1).

b) Fine Structure

Rb-Halides

Rb^+ 3d-transitions

The transitions from the Rb^+ 3d-subshell, which have their onset at about 110 eV, exhibit considerable fine structure, shown in Figs. 2 (for RbF), 3 (for RbCl), and 4 (for RbBr) and labeled B_d^+, C_d^+, ... The positions of these peaks are listed in Table III. The corresponding spin-orbit splitting can be estimated to be 1.67 eV by interpolation between the values calculated by Herman and Skillman for Kr (1.4 eV) and Sr (1.96 eV).[45] The actual value of the 3d spin-orbit splitting of Rb may actually be smaller: the value experimentally determined for gaseous Kr by Codling and Madden[46] is 1.22 eV, 0.18 eV smaller than the calculated one. We shall therefore reduce the calculated spin-orbit splitting of Rb by 0.18 eV, thus obtaining an estimate of 1.5 eV. An inspection of the peak positions listed in Table III suggests that the pairs (B_d^+, C_d^+), (D_d^+, E_d^+), and perhaps (F_d^+, Gd^+), with a separation of about 1.5 eV, are spin-orbit mates. The same conclusion applies to the (B_d^+, C_d^+) and (D_d^+, E_d^+) pairs of RbBr. In RbF the peaks observed are much broader ($\sim$ 3 eV width) than for RbCl and RbBr and hence the spin-orbit structure is not resolved. The reason for the larger width in RbF is not clear, but it may be related to a greater amount of crystalline disorder associated with the higher melting point of the material (775° C for RbF, 715° C for RbCl, 682° C for RbBr, 642° C for RbI[47] the substrates were kept at room temperature during the evaporation) or with the highly hygroscopic character of RbF. No structure related to the Rb 3d-levels has been observed in the 110 - 120 eV region for RbI. This fact is undoubtedly due to the strength

of the I^- 4d-continuum. The strength of the Rb 3d-transitions should be weak with respect to the continuum and at the same time their line width should be large because the Rb 3d-transitions must occur at the high energy side of the maximum in the continuum. This last fact provides a decay channel with a high density of states.

While the identification of spin-orbit mates given above is rather plausible, any further steps towards interpreting the fine structure of Figs. 2 - 5 must be taken, at present, on rather shaky grounds. The first question that one must consider is whether the structure can be interpreted in terms of one-electron band theory (density of conduction states x oscillator strength) or whether it is necessary to invoke many-body effects such as exciton interaction. It is known that final state Coulomb interaction between excited electron and hole left behind can play an important role in determining the absorption structure due to valence electrons, especially at the fundamental edge but also at higher energies.[48,49] In the case of metals, such interaction is responsible for the sharp structure observed for transitions from core levels to the Fermi surface.[50]

The width of the lines shown in Figs. 2 - 5 (the same conclusion applies to fine structure discussed later) is of the order of the width of structure in the one-electron density of states ($\sim$ 1 eV)[51] and hence it is highly questionable whether the exciton interaction plays a significant role in determining the experimental spectra Unfortunately, while a large number of band structure calculations have been performed for the alkali halides,[15-20] density of states, let alone matrix

elements for core transitions, are yet to appear. A comparison of such calculations with the experimental data should solve the question of the significance of exciton interaction in determining the line shapes. We should point out that Klima[51] has calculated X-ray emission spectra for Si (1s, 2p) and Ge (1s, 2p, 3p) and found good agreement with experiments. Evidence of excitonic effects has been obtained in NaCl from energy distribution measurements of photoemitted electrons excited from the Na^+ 2p shell.[52]

We shall make a coarse attempt, however speculative, to assign observed structure to critical points in the calculated conduction bands. Such an assignment would remain valid in the presence of exciton interaction provided such interaction does not scramble completely the calculated bands and one can talk still of excitons "tied" to certain interband critical points. Our work can be put on slightly firmer grounds by taking into account the ionic composition of the wave functions of the various band states, given by Onodera for KI[53] and CsI[19] (it is reasonable to assume it doesn't vary much for materials of the same structure).

For this purpose we show in Fig. 11 the band structure of RbBr calculated by Kunz.[16] The bottom of the conduction band, having s-character, should not give significant interband structure for transitions from d-levels. One may expect, at most, a weak forbidden exciton if the Coulomb interaction mixes a significant amount of p-like wave functions.[40] Such "forbidden" exciton is not seen for the Rb 3d-structure but may be the weak A_d peaks discussed later for Cs and Br, and I.

Figures 3 and 4 show two well defined groups of peaks associated with the Rb^+ 3d structure: (B_d^+, C_d^+) and (D_d^+, E_d^+, F_d^+) the separation between the centers of mass of both groups is about 4 eV, equal to the separation between the X_4' and X_5' states of Fig. 11. These states are composed of an admixture of p wave functions of both constituent atoms, with a slight predominance of the metallic component. Hence it is not unreasonable to assign the two groups of structure to these conduction states or to averages of the bands around these states produced by exciton interaction.

Transitions from the halogen ion

Fine structure, obviously related to the Br^- 3d levels, is seen in Fig. 4 between 70 and 80 eV. This structure is very similar to that observed for KBr.[42] While Fig. 5 does not show any Rb^+-related structure, it shows structure related to the 4d levels of I^- between 50 and 60 eV. This structure also has a striking similarity with that reported for KI.[42] As usual, we dispose first of the relatively simple question of the spin-orbit splitting. The spin-orbit splitting of the 4d levels of I, derived by interpolation between the calculated values[45] for Xe (2.15 eV) and Te (1.59 eV), is 1.87 eV. We lower this value to 1.7 eV because of the discrepancy between the calculated and the experimental (1.93 eV) splitting of Xe.[46] Similar procedure yields a splitting of about 1.0 eV for the 3d levels of Br^-. We thus find plausible the identification of the pairs (A_d^-, B_d^-), (C_d^-, D_d^-), (E_d^-, F_d^-) of RbBr and (B_d^-, D_d^-), (C_d^-, E_d^-), (G_d^-, H_d^-) of RbI as spin-orbit mates. The weak (A_d^-, B_d^-) pair of RbBr and the A_d^- line of RbI are suggestive of a forbidden exciton tied to the Γ_1 conduction band minimum. The stronger

structure in Fig. 4 between 70 and 80 eV can also be subdivided into two groups: (C_d^-, D_d^-) and (E_d^-, F_d^-, G_d^-), with a separation of about 4 eV. This fact is also suggestive of an origin related to the X_4' - X_5' states of Fig. 11. Similar identification,while not so clear, is also possible in Fig. 5.

We have already mentioned the similarity of the Br^- 3d- and I^- 4d-peaks of Rb and K Halides. A close similarity also appears in the conduction band structures calculated for KBr and RbBr[16], KCl[54] and RbCl[16], KF and RbF[15], and, to a lesser extent, KI and RbI[17]. The conduction band structures of the corresponding Na and Li halides are considerably different.[15,16,54-56] Such differences must be due, at least in part, to the absence of d-states in the cores of Na and Li, which affects the orthogonalization of the d-like conduction electrons. Those similarities also appear in the Cl^- 2p-transitions of KCl and RbCl (at about 200 eV)[57] and in the F^- 1s-transitions of KF and RbF (at about 680 eV)[58]; the corresponding spectra of the Li, Na, and Cs halides are quite different. The differences in the Cs halides may be attributed, except for CsF, to the different crystal structure. A close similarity in the spectra of the K and Rb halides also appears for the valence band transitions.[9]

Cs-Halides

The fine structure of the 4d-spectra of the Cs-halides is shown in Figs. 6 - 9 and their inserts. That of the 3p-transitions of Cs^+ is shown in Fig. 10.

Cs^+ 4d-transitions

The transitions from the Cs^+ 4d-subshell shown in Figs. 6 - 9 have their onset at approximately 80 eV. This structure shows less detail than the Rb^+ 3d-transitions, probably because of the stronger related d→f continuum of Cs^+. Three strong peaks (B_d^+, C_d^+, F_d^+) are seen, together with a certain amount of weaker structure. For a tabulation of the peak energies, see Table IV. With the usual procedure, we estimate the spin-orbit splitting of the Cs^+ 4d-levels to be 2.3 eV. Hence the B_d^+, C_d^+ pair of CsF (2.7 eV), CsCl (2.2 eV), CsBr (2.1 eV), and CsI (2.1 eV) can be identified as spin-orbit mates. A mate for the F_d^+ peak cannot be found unambiguously. The splitting between the B_d^+ and F_d^+ peak may be susceptible of an interpretation similar to that given for the Rb^+ 3d-peaks but not enough information about the ionic composition of the X states is available to make a detailed identification. The weak A_d^+ peaks may be related to "forbidden" excitons tied to Γ_1.

It is interesting to point out that the (A_d^+, B_d^+, ...) peaks move to higher energies in going from CsI to CsCl, as usual. However, the next step, that to CsF, brings a decrease in energy which must be related to the different crystal structure of CsF (rock salt, FCC) and the remaining Cs halides (SC). It has been also shown that the fundamental edge of CsCl[21], CsBr, and CsI[59] occurs at lower energy when crystallized in the metastable rock salt structure.

An interesting feature of the optical structure in Figs. 5 - 9 is the I_d^+, J_d^+ peaks at about 93 and 96 eV. Similar, although weaker structure has been observed ∿ 15 eV above the 4d threshold of Xe.[40] It has been interpreted as a double excitation: a 4d-core-electron and a 5p-valence

-electron of Cs^+ are excited simultaneously by a photon. The threshold for the 5p-excitation of Cs^+ is 13.0 eV[30,31], thus the structure at 92 - 96 eV could be attributed to this mechanism. It is not clear, however, whether the strength of the I_d^+ and J_d^+ peaks can be accounted for theoretically with double excitations.[60,61]

Transitions from the halogen ion

RbBr and RbI (Figs. 8 and 9) show structure due to Br^- 3d- and I^- 4d-levels. This structure is considerably less clear than the corresponding structure of the Rb-halides, due, at least in part, to the strong d→f continuum of Cs. Also, only the B_d^-, C_d^-, and D_d^- peaks are seen in CsBr: higher energy peaks associated with Br^- 3d should fall under the strong B_d^+, C_d^+, F_d^+ peaks of Cs^+ 4d. The energy difference between the C_d^- and E_d^- peaks of CsI is 1.8 eV, and hence it is possible to interpret them as a spin-orbit pair. The energies of the B_d^- and C_d^- peaks of CsBr also differ by 1.1 eV, close to the Br^- 3d-spin-orbit splitting. An unambiguous assignment of these peaks to a spin-orbit doublet is not possible since about the same splitting separates peaks C_d^- and D_d^-.

Cs^+ 4p-transitions

Towards the end of the high energy range of Figs. 6 - 9 (∿ 160 eV) a peak is seen (A_p^+) which can be assigned to transitions from the 4p subshell of Cs^+. This peak should have a spin-orbit-split mate with a splitting of about 13 eV, according to the calculations of Herman and Skillman[45] for Xe (11.5 eV) and Ba (14.2 eV). The most likely candidate for the spin-orbit mate of A_p^+ is peak F_p^+ of Fig. 10, which appears for

all materials and yields an average spin-orbit-splitting of 11.3 eV. The calculation of Herman and Skillman seems also to overestimate the spin-orbit-splitting of the 4p-states of Cs. We are not, at present, in a position to try to identify the remaining structure associated with these transitions shown in Fig. 10 (B_p^+, C_p^+, D_p^+, ...).

ACKNOWLEDGMENTS

The authors are grateful to P. Rabe and G. Singmann for help in the sample preparation and parts of the alkali halide films. Thanks are also due to D. Michael and E.W. Weiner for technical assistance during the course of experiments.

Literature

1. R.S. Knox and K.J. Teegarden, in Physics of Color Centers, Ed. W.B. Fowler (Academic Press, 1968), p. 1
2. W.B. Fowler, in Physics of Color Centers, Ed. W.B. Fowler (Academic Press, 1968), p. 54
3. H. Philipp, E.A. Taft, and L. Apker, Phys.Rev. 120, 49 (1960)
4. S. Ballarro, A. Balzarotti, and V. Grasso, Phys.Letters 23, 405 (1966)
5. U. Gerhardt, and E. Mohler, phys.stat.sol. 18, K 45 (1966)
6. D. Fröhlich and B. Staginnus, Phys.Letters 28A, 738 (1969)
7. R. Hilsch and R.W. Pohl, Z. Phys. 59, 812 (1930)
8. G. Baldini and B. Bosacchi, Phys.Rev. 166, 863 (1968)
9. B. Bosacchi, Proc. Conf. "Optical Properties of Solids" Ed. E.D.Haidemenakis (Gordon & Breach, to be published)
10. G. Baldini and B. Bosacchi, phys.stat.sol. (in press)
11. M. Creuzburg, Z. Physik 196, 433 (1966)
12. M. Creuzburg, Dissertation Universität Hamburg, 1966
13. J.C. Phillips, Solid State Physics, Vol. 18, Ed. F. Seitz and D. Turnbull, (Academic Press Inc., New York, N.Y. 1966), p. 55
14. C.W. Higginbotham, F.H. Pollak, and M. Cardona, Proc.Intern. Conf. on the Physics of Semiconductors, Moscow 1968, Vol. I, p. 57
15. A.B. Kunz, T. Miyakawa, and W.B. Fowler, to be published
16. A.B. Kunz, phys.stat.sol. 29, 115 (1968)
17. A.B. Kunz, J.Phys.Chem.Sol. 31, 265 (1970)
18. W.B. Fowler and A.B. Kunz, Phys.Rev. 186, 256 (1969)
19. Y. Onodera, J.Phys.Soc. Japan 25, 469 (1968)
20. U. Rössler, phys.stat.sol. 34, 207 (1969)
21. J.E. Eby, K.J. Teegarden, and D.B. Dutton, Phys.Rev. 116, 1099 (1959)
22. K. Teegarden and G. Baldini, Phys.Rev. 155, 896 (1967)

23. F. Fischer and R. Hilsch, Nachr. Akad. Wiss. Göttingen, II. Math. Phys. Kl. 8, 241 (1959)

24. G.R. Hugget and K. Teegarden, Phys.Rev. 141, 797 (1966)

25. R.S. Knox, Theory of Excitons (Academic Press, 1963), p. 38

26. G. Baldini, Phys.Rev. 128, 1562 (1962)

27. R. Haensel, G. Keitel, E.E. Koch, M. Skibowski, and P. Schreiber Phys.Rev. Letters 23, 1160 (1969)

28. R. Haensel, E.E. Koch, M. Skibowski, and P. Schreiber, DESY 69/51 (to be published)

29. J.C. Phillips, Phys.Rev. 136, A 1714 (1964)

30. H. Saito, S. Saito, R. Onaka and B. Ikeo, J.Phys.Soc. Japan 24, 1095 (1968)

31. C. Moore, NBS-Circular 467, Vol. I (1949), II (1958) and III (1958)

32. R. Haensel, C. Kunz, T. Sasaki, and B. Sonntag, Phys.Rev. Letters 20, 1436 (1968)

33. R. Haensel, C. Kunz and B. Sonntag, Phys.Rev. Letters 20, 262 (1968)

34. R.P. Godwin, Synchrotron Radiation as a Light Source, in Springer Tracts in Modern Physics, Vol. 51, Ed. G. Höhler (Springer Verlag 1969)

35. K. Siegbahn, C. Nordling, A. Fahlman, R. Nordberg, K. Hamrin, H. Hedman, G. Johansson, T. Bergmark, S.-E. Karlsson, I. Lingven und B. Lindberg, ESCA, Atomic, Molecular and Solid State Structure by Means of Electron Spectroscopy, Appendix I, (Almqvist Wiksells, Uppsala 1967)

36. R. Haensel and C. Kunz, Z. Angew. Phys. 23, 276 (1967)

37. R. Haensel, C. Kunz, T. Sasaki and B. Sonntag, Appl.Opt. 7, 301 (1968)

38. G. Sauerbrey, Z. Physik 155, 206 (1959)

39. The foils were purchased from Yissum Res.Dev.Comp., Tel-Aviv, Isreal

40. R. Haensel, G. Keitel, P. Schreiber, and C. Kunz, Phys.Rev. 188, (1969)

41. U. Fano and J.W. Cooper, Rev.Mod.Phys. 40, 441 (1968)

42. F.C. Brown, C. Gähwiller, H. Fujita, N. Carrera and W. Scheifley, Proc. X. European Congress for Molecular Spectroscopy, Liège 1969 (to be published)

43. H. Fujita, C. Gähwiller and F.C. Brown, Phys.Rev. Letters 22, 1369 (1969)

44. M. Cardona and R. Haensel, Phys.Rev. (in press)

45. F. Herman and S. Skillman, Atomic Structure Calculations (Prentice Hall, Inc., 1963)

46. K. Codling and R.P. Madden, Phys.Rev. Letters 12, 106 (1964)

47. Handbook for Chemistry and Physics (The Chemical Rubber & Co., Cleveland, Ohio, 49 nd Edition, 1968)

48. E.O. Kane, Phys.Rev. 180, 852 (1969)

49. J.C. Hermanson, Phys.Rev. 150, 660 (1966)

50. R. Haensel, G. Keitel, P. Schreiber, B. Sonntag, and C. Kunz Phys.Rev. Letters 23, 528 (1969) and Proc. NBS-Symposium "Electronic Density of States", Washington, D.C. 1969 (to be published) G.D. Mahan, Phys.Rev. 163, 612 (1967)

51. J. Klima, J.Phys.C. 3, 70 (1970) and private communication

52. R. Haensel, G. Keitel, G. Peters, P. Schreiber, B. Sonntag and C. Kunz, Phys.Rev. Letters 23, 530 (1970)

53. Y. Onodera, M. Okazaki, and T. Inui, J.Phys.Soc. Japan 21, 2229 (1966)

54. A.B. Kunz, Phys.Rev. 175, 1147 (1968)

55. A.B. Kunz, T. Miyakawa, and S. Oyama, phys.stat.sol. 34, 581 (1969)

56. A.B. Kunz, Phys.Rev. 180, 934 (1969)

57. Y. Iguchi et al., Sol.State Comm. 6, 575 (1968)

58. A.S. Vinogradov, T.M. Zimkina, and Y.F. Maltsev, Fiz. Tverd Tela 11, 3354 (1969)

59. A.A. Gavini and M. Cardona, Phys.Letters 27A, 112 (1968)

60. T. Miyakawa, J.Phys.Soc. Japan 17, 1898 (1962)

61. J.C. Hermanson, Phys.Rev. 177, 1234 (1969)

Table Captions

Table I Number of effective electrons N_{eff} obtained from our experimental absorption spectra with Eq (1) for the Rb and Cs halides. The range of integration (E_1-E_2) varies slightly for the various materials and is also listed.

Table II Contribution of the core transitions discussed in this paper to the refractive index of the Rb and Cs halides.

Table III Energy (in eV) of the peaks observed in the absorption spectra of the Rb halides at room temperature. The energy of the corresponding free atom levels[35] is also given.

Table IV Energy (in eV) of the peaks observed in the absorption spectra of the Cs halides at room temperature. The energy of the corresponding free atom levels[35] is also given.

Table I

Material	E_1 (eV)	E_2	N_{eff}
RbF	100	190	2,8
RbCl	100	190	1,3
BrBr	70	170	3,8
RbI	50	150	8,3
CsF	70	190	16,2
CsCl	70	190	15,1
CsBr	70	190	13,1
CsI	50	190	18

Table II

photon energy (eV)	$\Delta n \times 10^2$							
	RbF	RbCl	RbBr	RbI	CsF	CsCl	CsBr	CsI
60				1,3				2,3
70				1,5				2,6
80			0,3	1,0	4,0	3,7	2,2	2,5
90			0,3	0,2	4,5	3,9	2,2	1,8
100		0,2	0,3	-0,4	2,2	1,8	1,2	0,2
110	0,3	0,1	0,2	-0,8	-1,0	-0,7	-0,2	-1,4
120	0,2	0,1	0,1	-0,7	-2,3	-2,1	-0,9	-2,0
130	0,1	0,1	0,0	-0,6	-2,3	-2,4	-0,9	-1,9
140	0,1	0,0	-0,1		-2,0	-1,9	-0,8	-1,5
150	0,0	0,0	-0,2		-1,6	-1,5	-0,7	-1,2
160	-0,2	-0,1	-0,3		-1,4	-1,2	-0,6	-0,9
170	-0,2	-0,1			-1,3	-1,0	-0,6	-0,8
180						-0,9	-0,6	-0,6

Table III

		Free Atom	RbF		RbCl		RbBr		RbI	
I	$N_{IV,V}$	50								
									A_d^-	51,7±0,1
									B_d^-	52,7±0,1
									C_d^-	53,4
									D_d^-	54,4
									E_d^-	55,0
									F_d^-	56,2
									G_d^-	58,1
									H_d^-	59,6
									I_d^-	64
Br	M_V	69								
	M_{IV}	70								
							A_d^-	71,1		
							B_d^-	72,1±0,2		
							C_d^-	73,0±0,2		
							D_d^-	73,9±0,2		
							E_d^-	75,6±0,3		
							F_d^-	76,7±0,2		
							G_d^-	78,2±0,2		
							H_d^-	82,9		
							I_d^-	85,2±0,4		
Rb	M_V	111								
	M_{IV}	112								
				B_d^+	114,2±0,4	B_d^+	114,0±0,4			
			B_d^+	115,5±0,4						
				C_d^+	115,6±0,3	C_d^+	115,8±0,2			
				D_d^+	117,8±0,3	D_d^+	117,4±0,2			
			D_d^+	118,4						
				E_d^+	119,2±0,2	E_d^+	118,8±0,2			
				F_d^+	120,9±0,2					
						G_d^+	122,0±0,1			
				G_d^+	122,3±0,2					
				H_d^+	123,9±0,2					

Table III (continued)

I	$N_{II,III}$	123		
			I_d^+	125,4±0,2
			J_d^+	130,0±0,1
			K_d^+	131,6
			L_d^+	135,0±0,5

Table IV

		Free Atom		CsF	CsCl	CsBr	CsI
I	$N_{IV,V}$	50					
			C_d^-				53,1±0,2
			E_d^-				54,9±0,3
			F_d^-				55,7±0,1
			I_d^-				60,8±0,4
			J_d^-				63,4±0,3
			K_d^-				66,4±0,5
			L_d^-				68,5±0,3
			M_d^-				71,8±0,5
Br	M_V	69					
	M_{IV}	70					
			B_d^-			72,6±0,1	
			C_d^-			73,7±0,1	
			D_d^-			74,6±0,1	
Cs	N_V	77					
	N_{IV}	79					
			A_d^+	78,1±0,2	(78,7±0,2)		
			B_d^+	79,7±0,3	80,3±0,2	80,1±0,1	79,9±0,3
			C_d^+	82,4±0,3	82,5±0,2	82,2±0,1	82,0±0,4
			D_d^+	83,5			
			E_d^+	84,7±0,3			
			F_d^+	85,7±0,2	85,2±0,2	85,1±0,2	84,4±0,5
			G_d^+	87,5±0,2	88,7±0,3	88,2±0,2	
			H_d^+		(91,3)		
			I_d^+	92,8±0,2	93,2	93,2±0,2	(92,5±0,4)
			J_d^+	95,8±0,2	96,1	96,2±0,5	96,3±0,1
			K_d^+		101,1	102,8±0,3	100,7±0,4
			L_d^+			110,0±0,4	105,3±0,4

Table IV (continued)

Cs	N_{III}	162				
	N_{II}	172				
			A_p^+	161,6±0,2	161,7±0,4	161,7±0,4	161,7±0,4
			B_p^+	164,3±0,2	164,4±0,4		
			C_p^+	166,9±0,2	167,0±0,3		167, ±0,4
			D_p^+	168,5±0,2	169,5±0,3		
			E_p^+	170,7±0,2	170,9±0,3		170,8±0,4
			F_p^+	172,7±0,3	173,2±0,4	172,6±0,4	173,2±0,4
			G_p^+		176,7±0,3	176	
			H_p^+	183,0±0,3	185,8±0,4		180,9±0,5
			A_p^-			184,4±0,4	
			B_p^-			191,1±0,6	

Figure Captions

Fig. 1 Schematic diagram of the core energy levels of the Rb and Cs halides relevant to our photon energy region.

Fig. 2 Absorption spectrum of RbF from 90 eV to 190 eV. All measurements in this and subsequent figures were performed at room temperature.

Fig. 3 Absorption spectrum of RbCl from 90 eV to 190 eV.

Fig. 4 Absorption spectrum of RbBr from 70 eV to 170 eV.

Fig. 5 Absorption spectrum of RbI from 50 eV to 150 eV.

Fig. 6 Absorption spectrum of CsF from 70 eV to 170 eV.

Fig. 7 Absorption spectrum of CsCl from 70 eV to 170 eV.

Fig. 8 Absorption spectrum of CsBr from 70 eV to 170 eV.

Fig. 9 Absorption spectrum of CsI from 50 eV to 170 eV.

Fig. 10 Absorption spectra of the Cs-halides in the region of Cs^+ 4p-transitions.

Fig. 11 Band structure of RbBr according to A.B. Kunz (see Ref. 16).

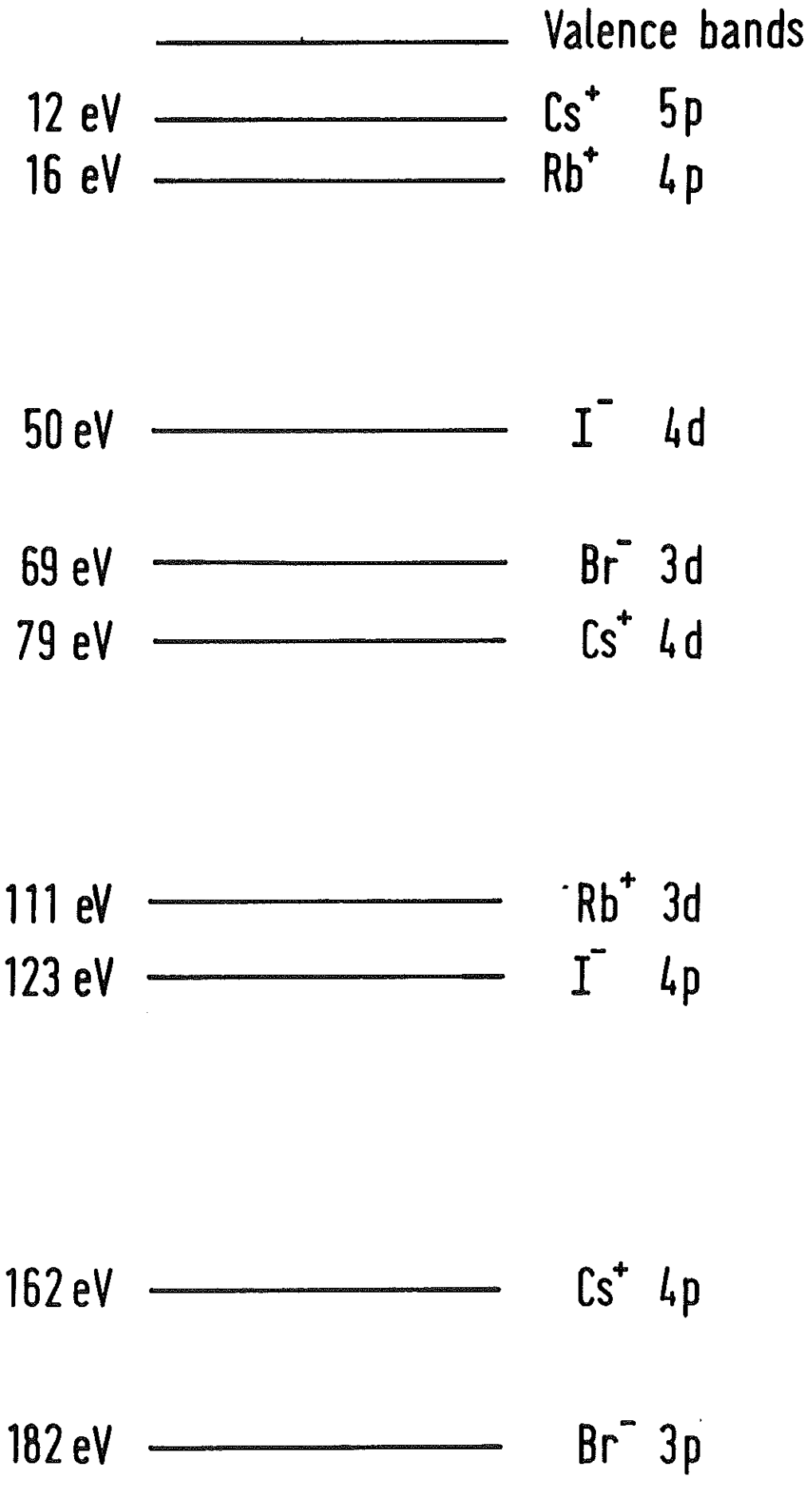
Valence bands
12 eV
Cs+ 5p
16 eV
Rb+ 4p
50 eV
I- 4d
69 eV
Br- 3d
79 eV
Cs+ 4d
111 eV
Rb+ 3d
123 eV
I- 4p
162 eV
Cs+ 4p
182 eV
Br- 3p

Fig.1

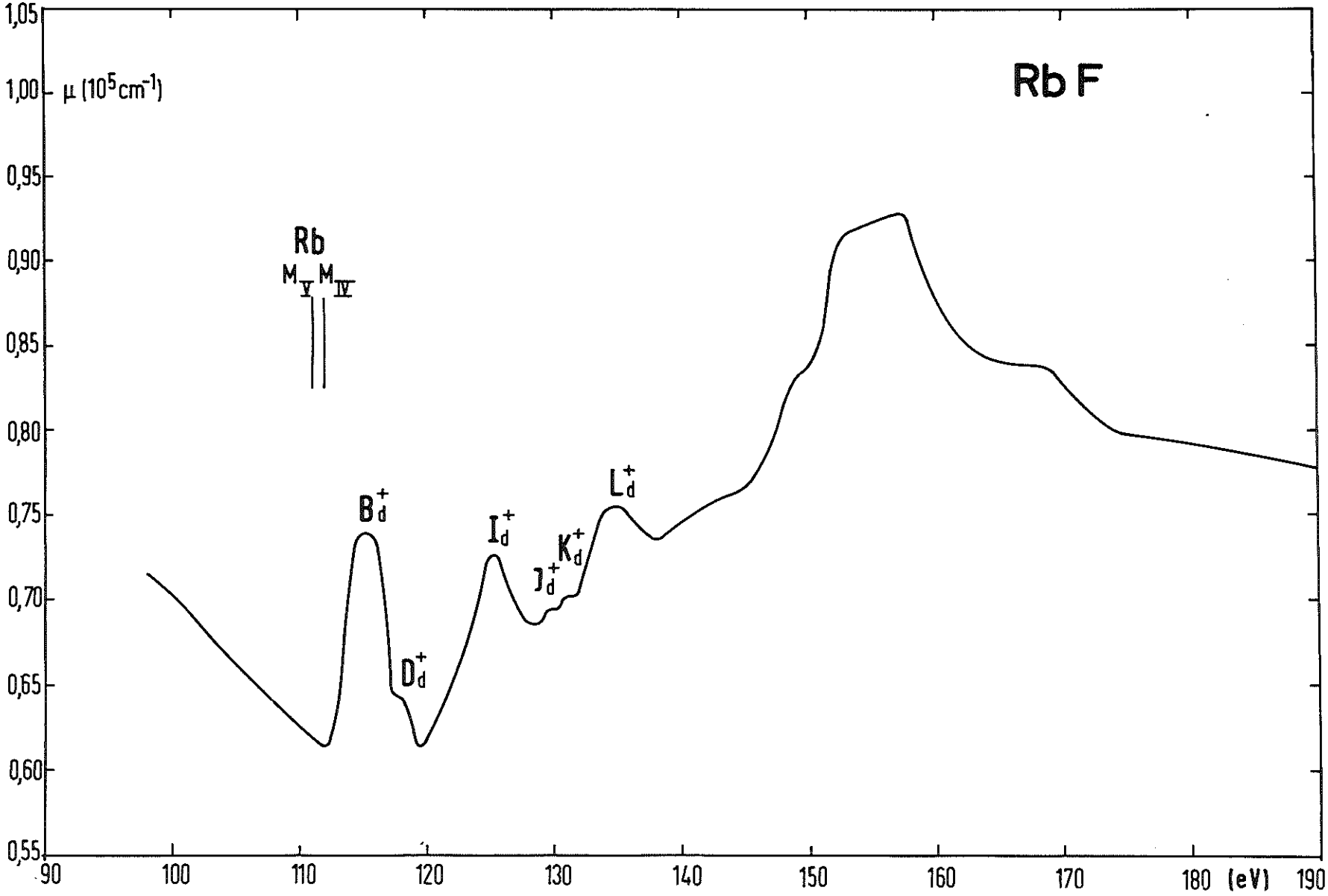
Rb F
μ (10⁵cm⁻¹)
1,05
1,00
0,95
0,90
0,85
0,80
0,75
0,70
0,65
0,60
0,55
Rb
M_V M_IV
B_d^+
D_d^+
I_d^+
J_d^+
K_d^+
L_d^+
90
100
110
120
130
140
150
160
170
180
(eV)
190

Fig.2

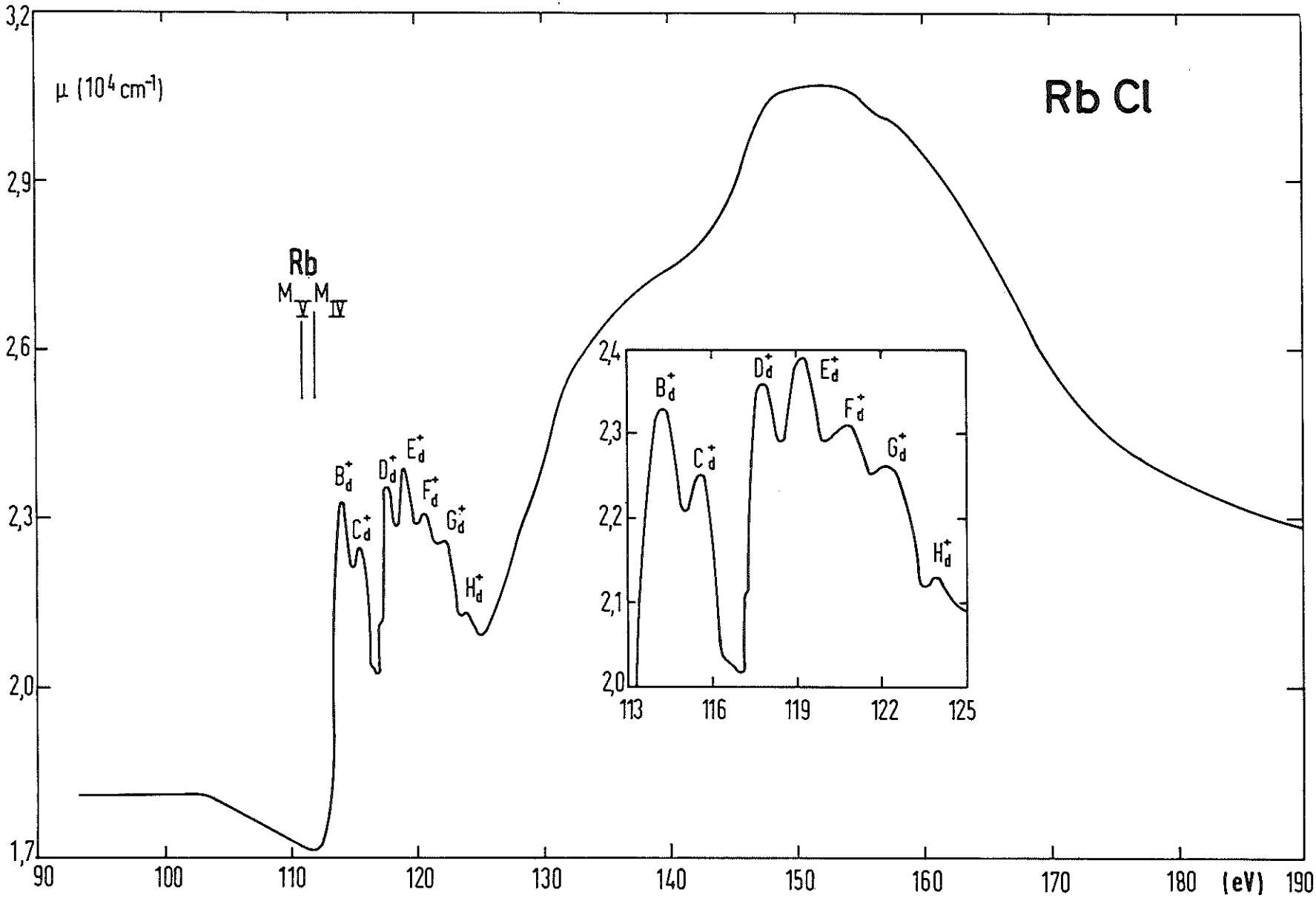
Rb Cl
μ (10⁴ cm⁻¹)
Rb
M_V M_IV
B_d⁺
C_d⁺
D_d⁺
E_d⁺
F_d⁺
G_d⁺
H_d⁺
3,2
2,9
2,6
2,3
2,0
1,7
90
100
110
120
130
140
150
160
170
180
(eV)
190
2,4
2,3
2,2
2,1
2,0
113
116
119
122
125

Fig.3

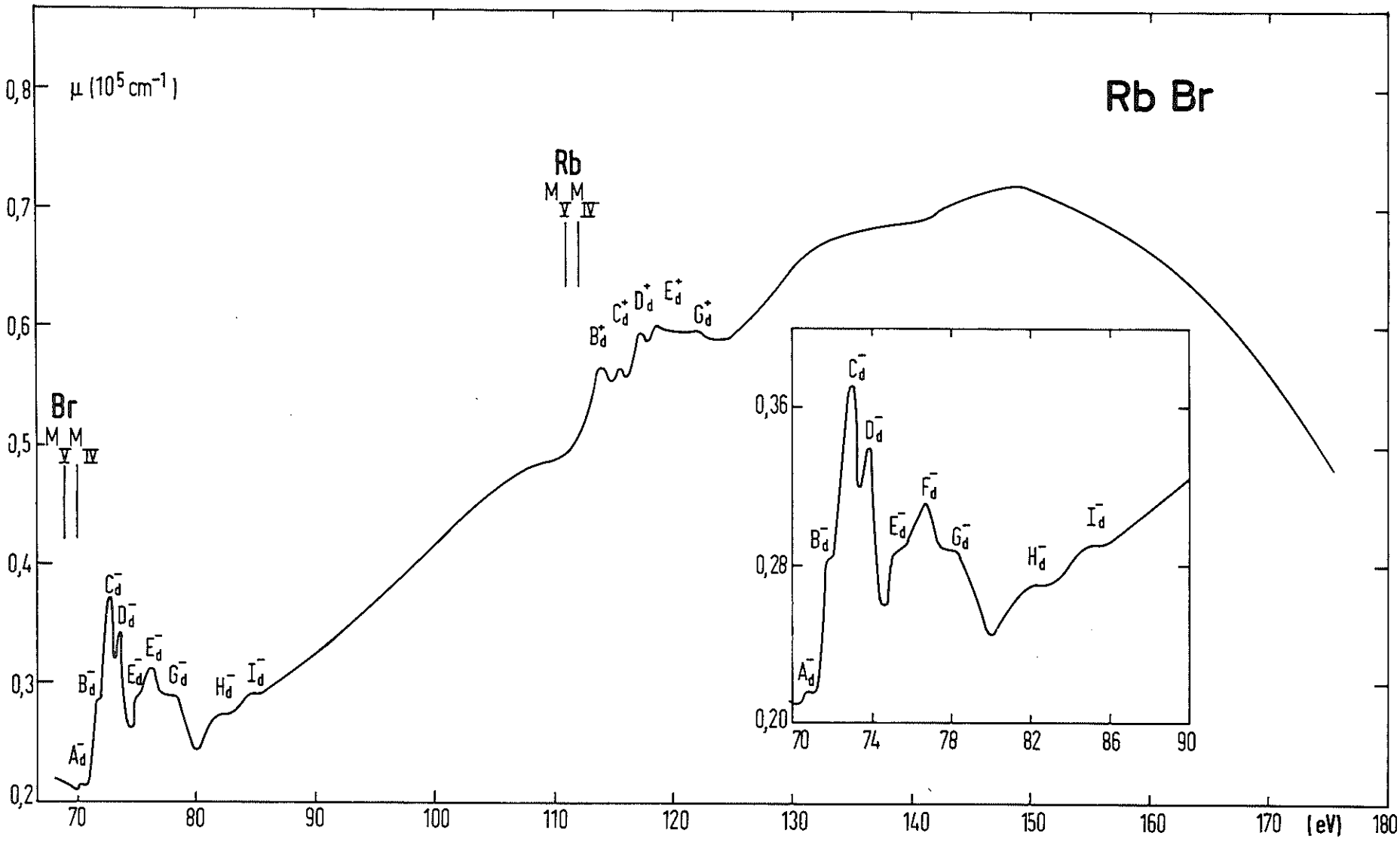
Rb Br
μ (10⁵ cm⁻¹)
Br
M V M IV
Rb
M V M IV
A⁻d
B⁻d
C⁻d
D⁻d
E⁻d
E⁻d
G⁻d
H⁻d
I⁻d
B⁺d
C⁺d
D⁺d
E⁺d
G⁺d
0,8
0,7
0,6
0,5
0,4
0,3
0,2
70
80
90
100
110
120
130
140
150
160
170
(eV)
180
0,36
0,28
0,20
74
78
82
86

Fig.4

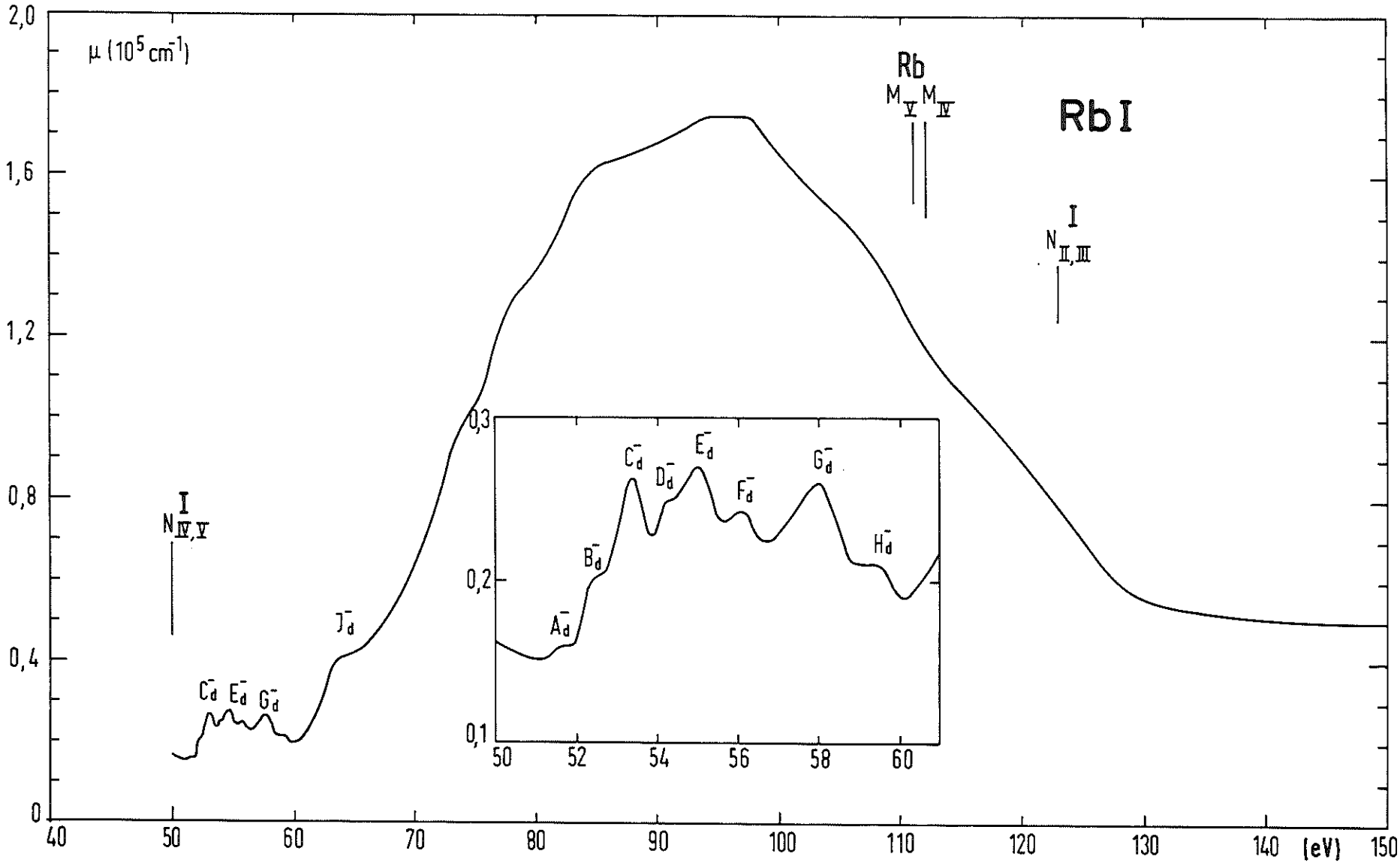
μ (10⁵ cm⁻¹)
Rb
M_V M_IV
RbI
I
N_II,III
I
N_IV,V
C_d⁻ E_d⁻ G_d⁻
J_d⁻
A_d⁻ B_d⁻ C_d⁻ D_d⁻ E_d⁻ F_d⁻ G_d⁻ H_d⁻
2,0
1,6
1,2
0,8
0,4
0
0,3
0,2
0,1
40 50 60 70 80 90 100 110 120 130 140 (eV) 150
50 52 54 56 58 60

Fig. 5

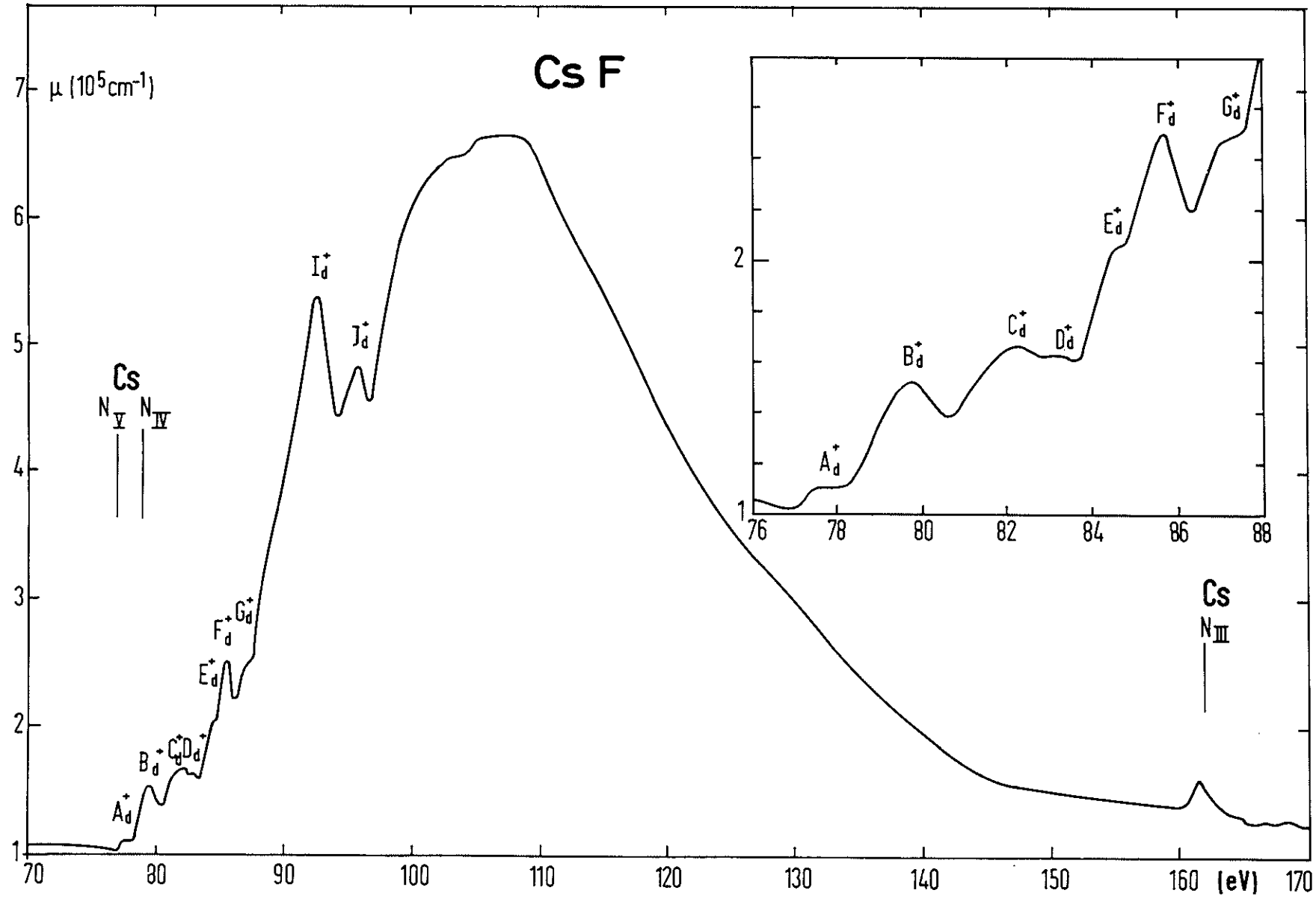

Fig.6

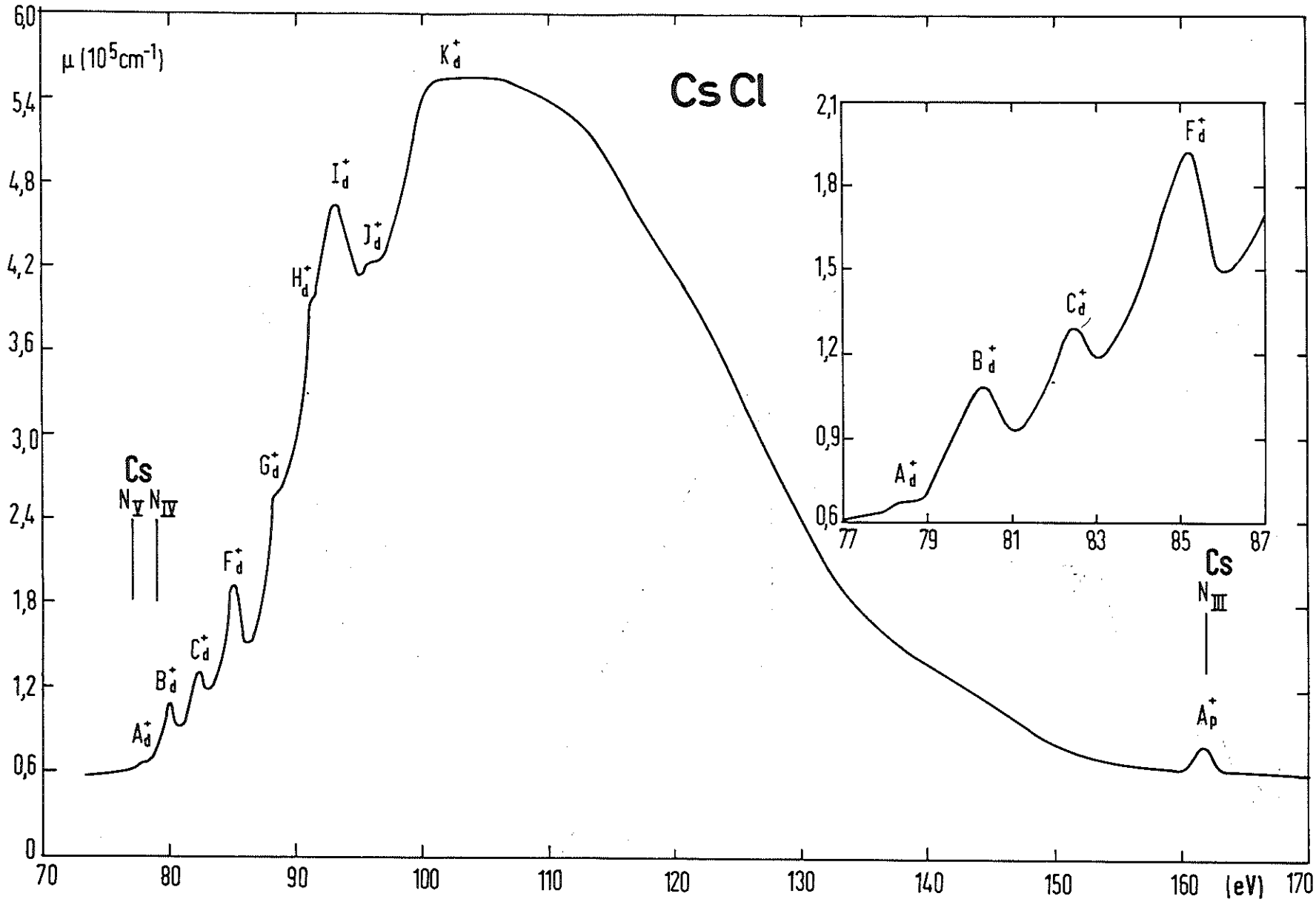

Fig. 7

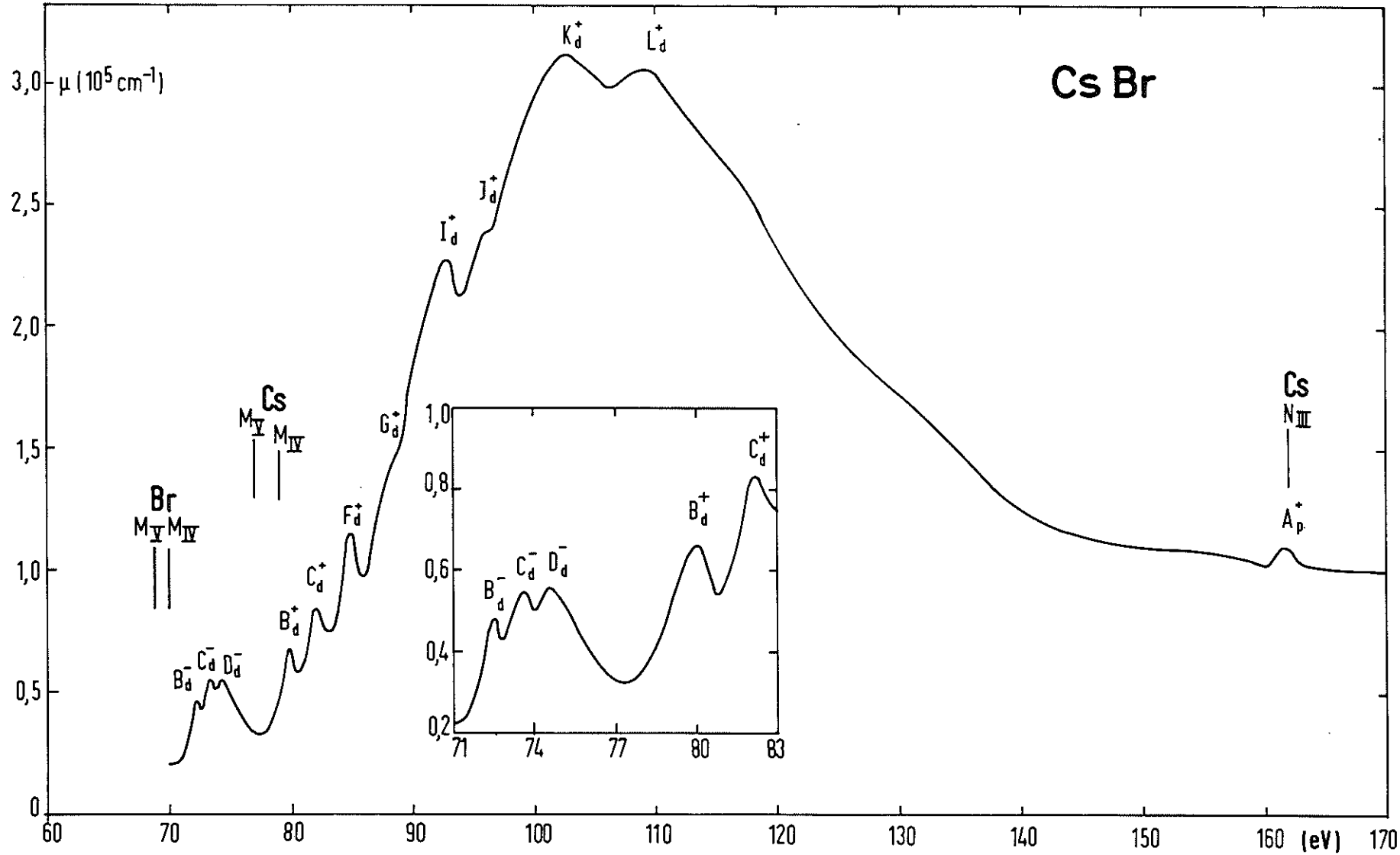
Cs Br
μ (10⁵ cm⁻¹)
3,0
2,5
2,0
1,5
1,0
0,5
0
60
70
80
90
100
110
120
130
140
150
160
170
(eV)
K_d^+
L_d^+
J_d^+
I_d^+
G_d^+
F_d^+
C_d^+
B_d^+
B_d^- C_d^- D_d^-
Br
M_V M_IV
Cs
M_V M_IV
Cs
N_III
A_p^+
1,0
0,8
0,6
0,4
0,2
71
74
77
80
83

Fig.8

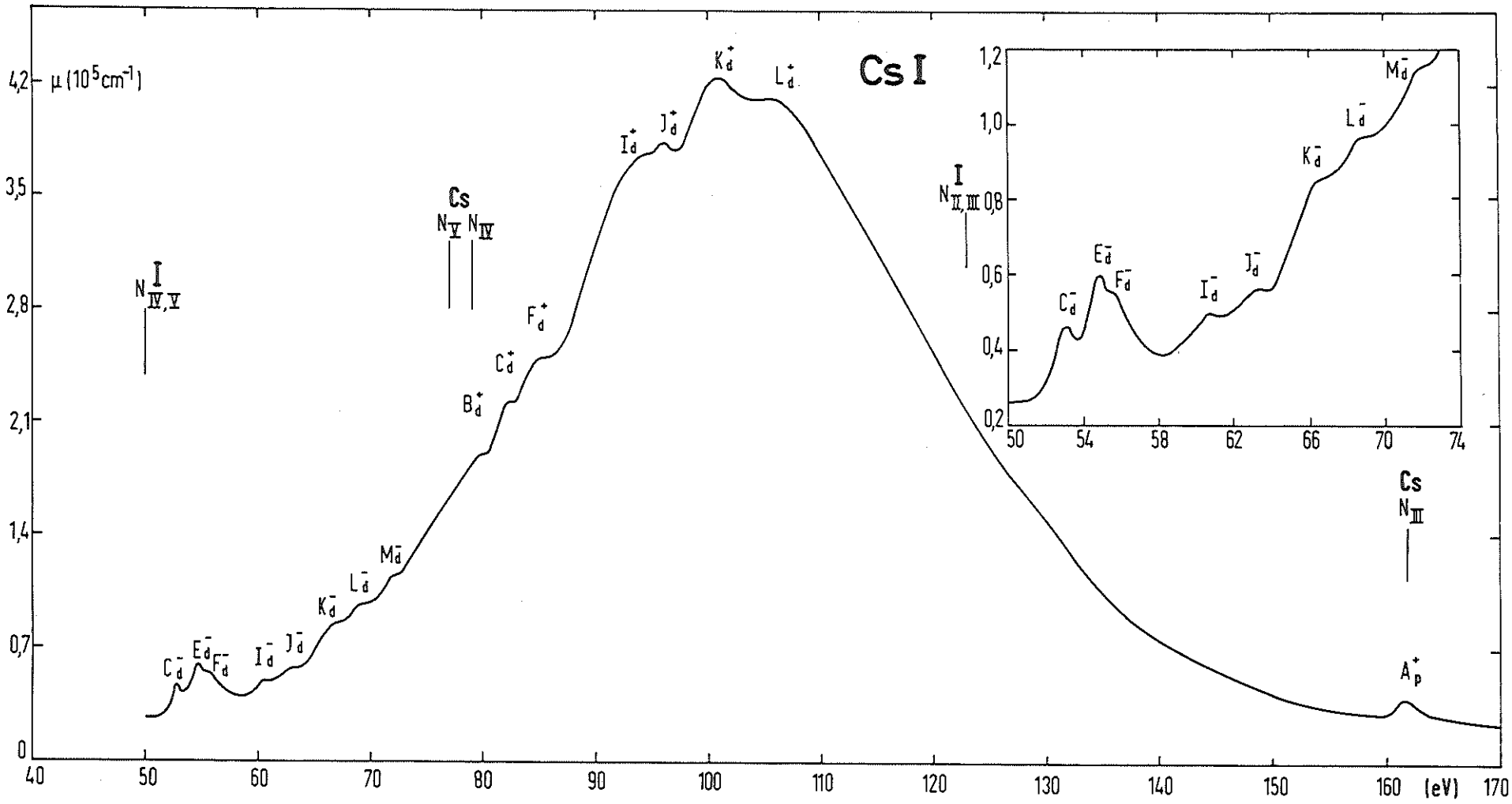
Cs I
μ (10⁵cm⁻¹)
4,2
3,5
2,8
2,1
1,4
0,7
0
40
50
60
70
80
90
100
110
120
130
140
150
160
170
(eV)
N I IV,V
Cs N V N IV
Cs N III
C⁻d
E⁻d
F⁻d
I⁻d
J⁻d
K⁻d
L⁻d
M⁻d
B⁺d
C⁺d
F⁺d
I⁺d
J⁺d
K⁺d
L⁺d
A⁺p
N I II,III
1,2
1,0
0,8
0,6
0,4
0,2
50
54
58
62
66
70
74

Fig. 9

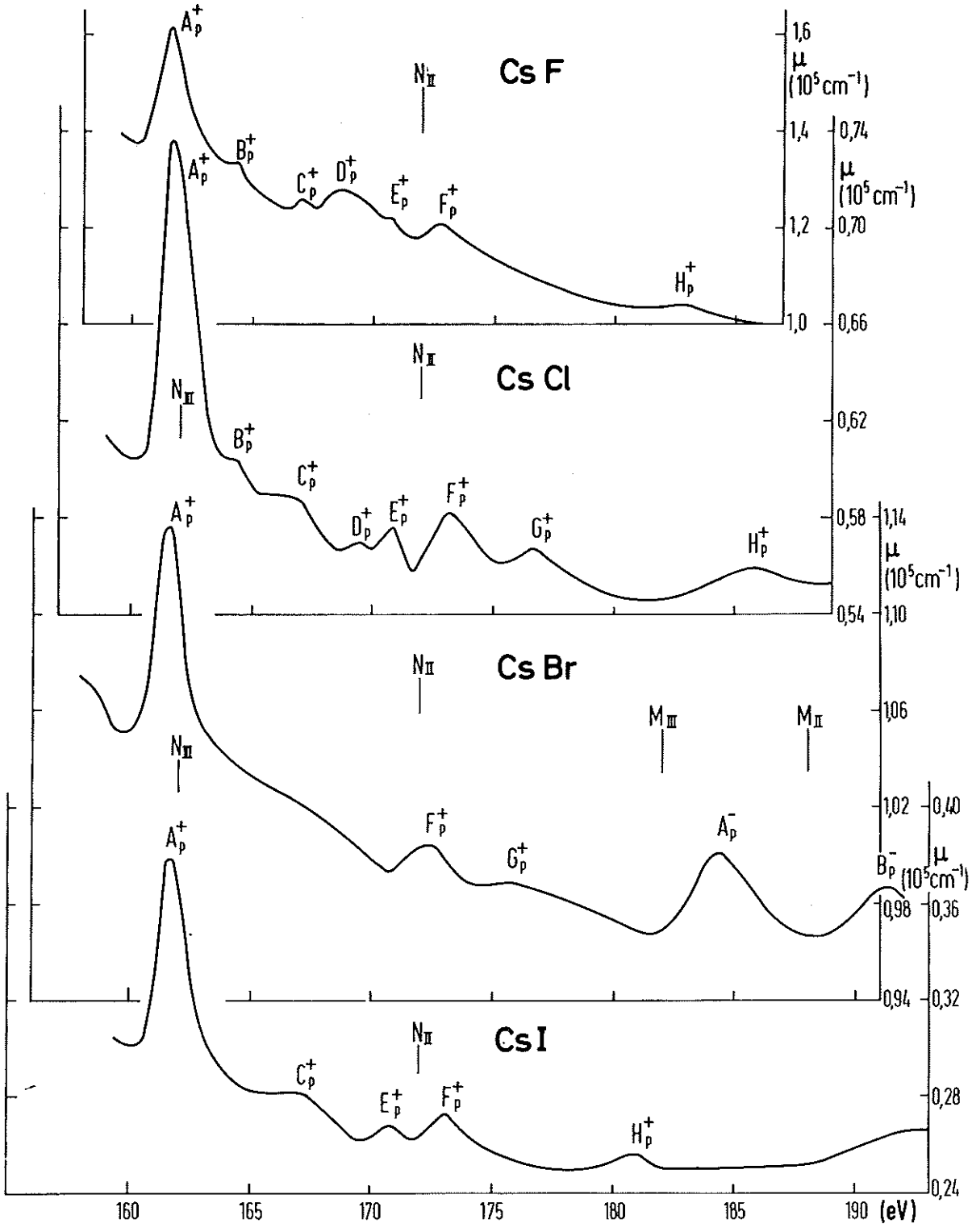
Cs F
Cs Cl
Cs Br
Cs I
A_p^+
B_p^+
C_p^+
D_p^+
E_p^+
F_p^+
G_p^+
H_p^+
A_p^-
B_p^-
N_{II}
N_{III}
M_{III}
M_{II}
μ ($10^5 cm^{-1}$)
1,6
1,4
1,2
1,0
0,74
0,70
0,66
0,62
0,58
0,54
1,14
1,10
1,06
1,02
0,98
0,94
0,40
0,36
0,32
0,28
0,24
160
165
170
175
180
185
190 (eV)

Fig. 10

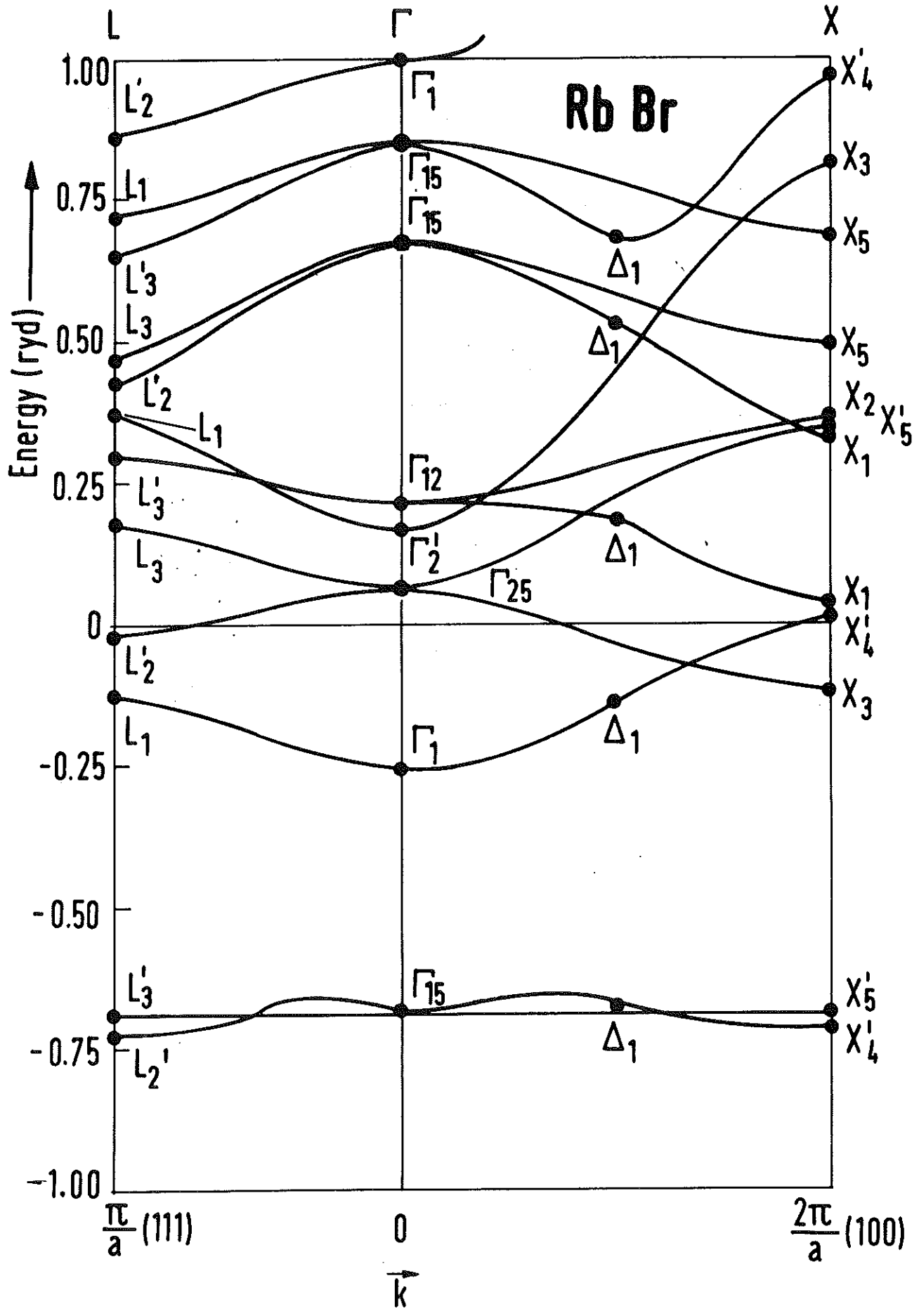
L
Γ
X
Rb Br
Energy (ryd)
1.00
0.75
0.50
0.25
0
-0.25
-0.50
-0.75
-1.00
L'2
L1
L'3
L3
L'2
L1
L'3
L3
L'2
L1
L'3
Γ1
Γ15
Γ15
Γ12
Γ'2
Γ25
Γ1
Γ15
Δ1
Δ1
Δ1
Δ1
Δ1
X'4
X3
X5
X5
X2
X'5
X1
X1
X'4
X3
X'5
X'4
π/a (111)
0
2π/a (100)
k

Fig. 11